ORIGINAL PAPER

Fluorescence Investigation of Interactions Between Novel Benzanthrone Dyes and Lysozyme Amyloid Fibrils

Kateryna Vus · Valeriya Trusova · Galyna Gorbenko ·
Rohit Sood · Elena Kirilova · Georgiy Kirilov ·
Inta Kalnina · Paavo Kinnunen

Abstract A series of novel fluorescent benzanthrone dyes have been tested for their ability to identify and characterize fibrillar aggregates of lysozyme prepared by protein denaturation in concentrated ethanol solution (F_{eth}) or acidic buffer (F_{ac}). Quantitative parameters of the dye association with native and fibrillar protein have been derived from the results of fluorimetric titration. The binding characteristics proved to be different for F_{eth}- and F_{ac}-bound benzanthrones, highlighting the dye sensitivity to the distinctions in fibril morphology. By comparing the dye preference to fibrillar protein aggregates, AM2, A8 and A6 were selected as the most prospective amyloid tracers. Based on the analysis of red edge excitation shifts and fluorescence lifetimes of the amyloid-bound dyes it was assumed that surface grooves or dry "steric zipper" interface are potential fibril binding sites for the novel fluorophores.

Keywords Benzanthrone dyes · Amyloid marker · Fibrillar lysozyme · Polarity

K. Vus (✉) · V. Trusova · G. Gorbenko
Department of Biological and Medical Physics, V.N. Karazin
Kharkiv National University, 4 Svobody Sq, 61022 Kharkiv, Ukraine
e-mail: katenka_vus@mail.ru

R. Sood · P. Kinnunen
Department of Biomedical Engineering and Computational Science,
School of Science and Technology, Aalto University, Otakaari 3,
FI-00076 Espoo, Finland

E. Kirilova · G. Kirilov · I. Kalnina
Department of Chemistry and Geography, Faculty of Natural
Sciences and Mathematics, Daugavpils University, Vienibas 13,
LV5401 Daugavpils, Latvia

Introduction

It is becoming generally accepted that conformational disorders, such as Alzheimer's and Parkinson's diseases, hereditary amyloidosis, type II diabetes, etc., are characterized by accumulation of the insoluble highly ordered protein aggregates (amyloid fibrils) in various human tissues [1]. These aggregates are composed largely of misfolded proteins polymerized into amyloid fibrils sharing a core cross-β-sheet structure, in which polypeptide chains are oriented in such a way that β-strands run perpendicularly to the long axis of the fibril, while β-sheets propagate in its direction. In view of the dramatic role of protein pathological aggregates in the development of severe diseases, accurate detection and characterization of amyloid fibrils represent the focus of current research efforts [1, 2]. A good deal of analytical tools, such as transmission electron microscopy (TEM) [3], atomic force microscopy (AFM) [4, 5], circular dichroism (CD) [1, 3], dynamic light scattering (DLS) [6, 7] and spectroscopic methods [8] have been successfully employed to gain insight into fibril morphology and physicochemical properties. Of these, fluorescence spectroscopy seems to be one of the most informative techniques due to its inherent sensitivity and versatility, good spatial and temporal resolution [9]. A wide range of fluorescent probes, including classical amyloid marker Thioflavin T (ThT) [10, 11], molecular rotor 4-dicyanovinyl-julolidine (DCVJ) [12], 2-anilinonaphthalene-6-sulfonate (ANS) and its derivatives [12, 13], Nile Red [14], Coumarin 6 [15], fluorinated styryl benzazoles [16], curcumin-derivatized probe CRANAD-2 [17], etc., have been developed to identify and characterize protein fibrillar aggregates. Although being prized for high specificity to different types of protein assemblies, these reporter molecules suffer from several drawbacks, particularly, rather high affinity for native proteins [14] or amorphous protein aggregates [15, 18], sensitivity to amino acid sequence [14], pH and ionic strength of bulk solution [14,

19], and ability to perturb fibril structure [6]. These pitfalls strongly suggest the necessity of designing the novel amyloid markers. Our previous studies revealed one prospective class of fluorescent probes—benzanthrone dyes (BD), highly sensitive to the oligomeric and fibrillar aggregates of lysozyme (HEWL) [20]. Moreover, these dyes possess several remarkable characteristics: i) low fluorescence intensity in buffer; ii) high Stokes shifts and extinction coefficients; iii) high sensitivity to environmental polarity [21]. Specifically, cumulative data from the binding and red edge excitation shift experiments allowed us to define fluorescence parameters reflecting the dye preference to either pre-fibrillar or fibrillar protein aggregates. Inspired by such unrivalled potential of BD in differentiating between the oligomeric and fibrillar protein assemblies, here we extend the investigation of BD amyloid sensitivity and address the question of whether BD are capable of distinguishing between morphologically different amyloid fibrils. More specifically, our goal was several-fold: (i) to evaluate the sensitivity of novel BD to fibrillar lysozyme, prepared either in concentrated ethanol solution or by acidic denaturation; (ii) to compare amyloid specificity of BD with that of ThT; iii) to characterize the properties of fibril-dye binding sites through red edge excitation shift (REES) analysis and fluorescence lifetime measurements.

Materials and Methods

Chemicals

Chicken egg white lysozyme (HEWL) was purchased from Sigma (St. Louis, MO, USA). Benzanthrone dyes (Fig. 1) were synthesized at the Faculty of Natural Sciences and Mathematics of Daugavpils University, as described previously [21]. Stock solutions of benzanthrones were prepared by dissolving the dyes in ethanol or dimethylsulfoxide.

Preparation of Lysozyme Fibrils

Amyloid fibrils of the first type (F_{eth}) were prepared by dissolving lysozyme (3 mg/ml) in deionized water with subsequent slow addition of ethanol to a final concentration 80 %. Next, the samples were subjected to a constant agitation at ambient temperature during 30 days [22]. Amyloid fibrils of the second type (F_{ac}) were obtained by incubation of lysozyme solution (10 mg/ml) in 10 mM glycine buffer (pH 2.2) at 60 °C during 6 days [23]. The amyloid nature of fibrillar aggregates was confirmed by TEM. Native lysozyme solution (3 mg/ml) in 5 mM sodium phosphate buffer was used as a control. A separate series of experiments were conducted to determine fluorescence lifetimes of the dyes in the presence of lysozyme fibrils prepared in acidic buffer.

Transmission Electron Microscopy

For electron microscopy assay, a 10 μl drop of the protein solution was applied to a carbon-coated grid and blotted after 1 min. A 10 μl drop of 2 % (w/v) uranyl acetate solution was placed on the grid, blotted after 30 s, and then washed 3 times by deionized water and air dried. The resulting grids were viewed at Jeol JSM-840 or Tecnai 12 BioTWIN electron microscope.

Steady-State Fluorescence Measurements

Steady-state fluorescence spectra of lysozyme in its native and fibrillar states were recorded with LS-55 (Perkin-Elmer Ltd., UK) or Varian Cary Eclipse (Varian Instruments, Walnut Creek, CA) spectrofluorimeters equipped with a magnetically stirred, thermostated cuvette holder. Fluorescence measurements were performed at 20 °C using 10 mm path-length quartz cuvettes. The excitation and emission slit widths were set at 10 nm. Excitation wavelengths and emission maxima of the examined dyes are given in Table 1. Quantum yields of fibril-bound dyes were calculated using the standard dye Rhodamine 101 (Q= 0.91 in acidified ethanol [24]), and allowing for the refractive indexes of amyloid fibrils ($n\sim1.5$ [25]) and ethanol ($n\sim1.36$).

Binding Model

Quantitative characteristics of the dye-lysozyme binding were determined in terms of the Langmuir adsorption model by analyzing protein-induced changes in the probe fluorescence intensity at the wavelengths, corresponding to emission maxima for each dye, as described previously [20]. Briefly, approximation of the experimental dependencies ΔI (fluorescence intensity increase) on C_P (total protein concentration) by Eq. 1 allowed us to determine the dye-protein binding parameters—association constant (K_a), binding stoichiometry (n) and molar fluorescence (α), characterizing the difference between molar fluorescence of the bound and free dye:

$$\Delta I = 0.5\alpha \left[Z_0 + nC_P + 1/K_a - \sqrt{(Z_0 + nC_P + 1/K_a)^2 - 4nC_P Z_0} \right] (1)$$

where Z_0 is the total probe concentration.

Time-Resolved Fluorescence Measurements

Time-resolved fluorescence intensity decays of benzanthrone dyes in dimethylformamide (DMF) and in the presence of F_{ac} were measured using a Photon Technology International spectrofluorometer equipped by GL-302 Dye Laser (Canada). This machine uses GL-3300 Nitrogen Laser that delivers a crisp pulse at 337 nm. The solution of LC 4230 (POPOP) laser dye (Kodak, USA) in a mixture of toluene with ethanol was used

Fig. 1 Structural formulas of aminobenzanthrone dyes
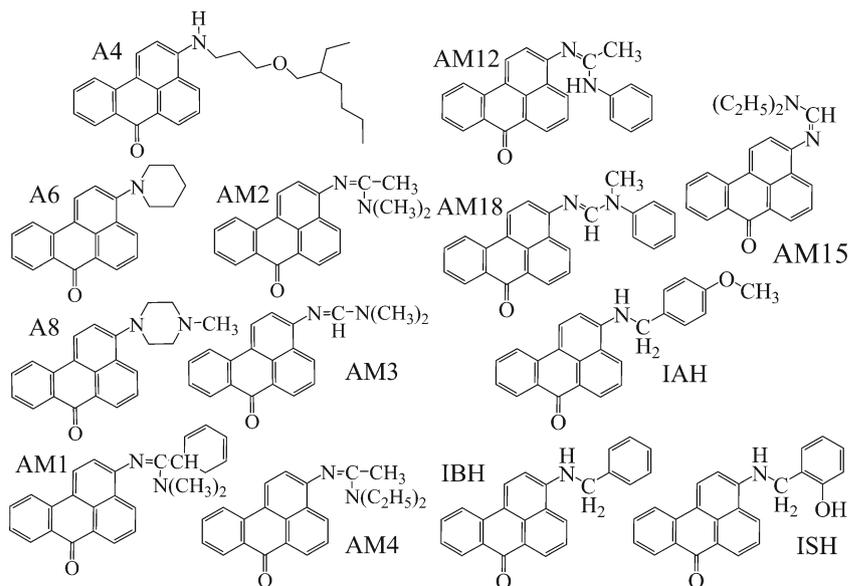
to excite benzanthrone dyes at 421 nm [26]. Instrument response functions were measured at the excitation wavelength using the colloidal silica (Ludox) as a scatterer. To optimize signal-to-noise ratio, 3,500 photon counts were collected in the peak channel. To get smooth curves the final decay profile of each dye was obtained as the average of 6 repeats. The resulted data were fitted by mono- (for the dyes in DMF) or biexponential (for the probes in the presence of F_{ac}) functions using Felix-GX software [9]:

$$I(t) = \sum_{i=1}^{n} \alpha_i \exp(-t/\tau_i) \qquad (2)$$

Table 1 Excitation (λ_{ex}) and emission ($\lambda_{em}^{F_{eth}}$, $\lambda_{em}^{F_{ac}}$) maxima of benzanthrone dyes and ThT in the presence of lysozyme fibrils prepared in concentrated ethanol solution (λ_{ex}, $\lambda_{em}^{F_{eth}}$) or by acidic denaturation (λ_{ex}, $\lambda_{em}^{F_{ac}}$)

Dye	λ_{ex}, nm	$\lambda_{em}^{F_{eth}}$, nm	$\lambda_{em}^{F_{ac}}$, nm
A4	490	630	645
A6	450	586	604
A8	440	583	580
AM1	450	593	586
AM2	450	575	582
AM3	450	575	586
AM4	470	580	603
AM12	469	578	576
AM15	475	577	571
AM18	465	565	571
IAH	523	594	621
IBH	524	602	626
ISH	531	605	628
ThT	420	480	488

where τ_i and α_i are decay times and pre-exponential coefficients, n is the number of fluorescence lifetime components, $i=1$ or 2 for monoexponential or biexponential decays, respectively.

The goodness of each fit was characterized by the value of reduced chi-square, weighted residuals and autocorrelation function of the weighted residuals [27]. A fit was considered good when χ^2 fell within the range of 0.8 to 1.2, and the plots of weighted residuals and autocorrelation function were randomly distributed around zero [9].

The fractional contributions (f_i) of each lifetime component to the steady-state intensity of the dyes in the presence of F_{ac} were calculated as follows [9]:

$$f_i = \frac{\alpha_i \tau_i}{\sum_{j=1}^{n} \alpha_j \tau_j} \qquad (3)$$

The average fluorescence lifetime ($<\tau>$) of the dyes in the presence of F_{ac} was calculated using the following Eq. 4:

$$<\tau> = f_1\tau_1 + f_2\tau_2 \qquad (4)$$

Results and Discussion

Binding Studies

To evaluate amyloid specificity of benzanthrones, at the first step of the study the dyes were titrated with F_{eth}, F_{ac} or native lysozyme. Figure 2 represents typical fluorescence spectra recorded upon BD titration with lysozyme fibrils. Fluorescence intensity of all dyes was found to increase with the protein concentration, suggesting that fluorophore is transferred into less polar environment [27, 28]. To derive the
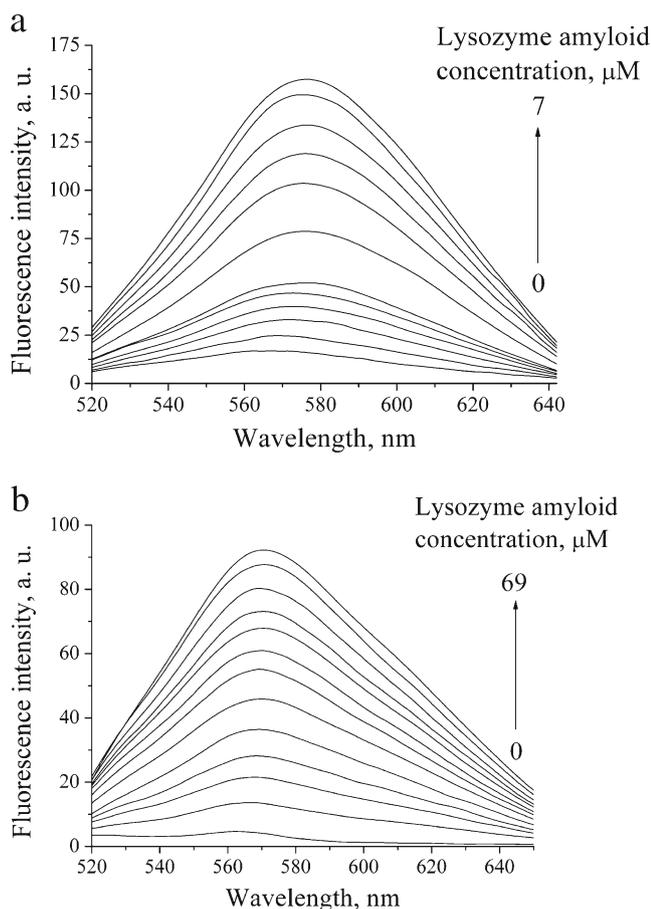
Fig. 2 Emission spectra of AM15 recorded upon the dye fluorimetric titration with F_{eth} (**a**) or F_{ac} (**b**). Dye concentration was 8.7 μM (**a**) and 0.8 μM (**b**)

Fig. 3 The isotherms of benzanthrone binding to F_{eth} (**a**) and F_{ac} fibrils (**b**). A8, AM1, AM2, AM12 and AM15 concentrations, μM, were: 1.6, 0.1, 0.1, 16.3, 8.7, respectively (**a**), and 1.3, 3.4, 20.2, 2.1, 0.8, respectively (**b**)

quantitative parameters of dye-protein complexation, the experimental dependencies of ΔI (C_P) (Fig. 3) were approximated by Eq. 1. As seen in Tables 2 and 3, three dyes, viz. A6, A8 and IBH possess similar fluorescence quantum yields (Q) when bound to F_{eth} and F_{ac} fibrils, while for the other benzanthrones this parameter turned out to be substantially higher in F_{eth} samples. Especially pronounced differences in the quantum yields of F_{eth}- and F_{ac}-bound dyes were found for AM1 (by a factor of *ca*. 10) and AM2 (by a factor of *ca*. 19). Remaining five dyes (A8, AM12, AM15, IAH, ISH) display the opposite behavior—their quantum yields are lower in F_{eth} fibrils compared to F_{ac}. Likewise, association constants and binding stoichiometries appeared to be different for F_{eth}- and F_{ac}-bound BD (Tables 2 and 3). In an attempt to rationalize these findings, we hypothesized that benzanthrones are sensitive to the differences in amyloid morphology. As seen in Fig. 4, lysozyme fibrils prepared by two different techniques involving organic solvent or low pH conditions, possess typical amyloid appearance, being rod-like, unbranched and devoid of amorphous material. However, F_{eth} and F_{ac} fibrils seem to differ in their molecular architecture, as judged from

the differences in their length (0.9 and 0.9–1.5 μm) and diameter (25±2 and 7±0.6 nm, respectively).

It is widely accepted that amyloid morphology is determined by the conditions of fibril growth [29, 30]. Specifically, distinctions between partially unfolded protein states formed under varying environmental conditions may be responsible for various fibril morphologies [31]. In the case of lysozyme, amyloid growth was assumed to be a two-stage cooperative process where denaturation of α-helix structures of the native protein precedes β-sheet formation [23]. The morphology of HEWL fibrils proved to be dependent on pH [29, 32], temperature [2, 33], ionic strength [2, 29], the presence of organic solvents [34, 35], agitation [22, 29], etc. In particular, in 80 % ethanol, at neutral pH and constant agitation, HEWL adopts a flexible, easily entangled "broken rod" conformation that

Table 2 Binding characteristics of benzanthrone dyes associated with lysozyme fibrils prepared in concentrated ethanol solution (F_{eth})

[a] Dye	K_a, μM^{-1}	n	I/I_0	I/I_{nat}	Q	[c] REES, nm
A4	2.9±0.7	0.2±0.04	5.2	3.7	0.07±0.015	7
A6	27±6	0.23±0.05	2.4	[b] –	0.43±0.11	6
A8	1.7±0.15	0.22±0.04	1.9	[b] –	0.52±0.12	14
AM1	2±0.4	0.22±0.04	5.7	[b] –	0.73±0.14	21
AM2	5±1	0.35±0.07	38.4	5.0	0.77±0.17	3.5
AM3	70±8	0.56±0.12	9.7	7.2	0.38±0.09	2
AM4	2.6±0.2	0.2±0.06	3.7	3.1	0.56±0.12	19.5
AM12	0.23±0.05	3.7±0.72	6.8	3.9	0.12±0.03	0
AM15	0.44±0.09	1.9±0.41	7.4	3.2	0.07±0.01	0
AM18	1.9±0.4	0.78±0.16	5.8	3.3	0.52±0.13	0
IAH	0.1±0.02	3±0.61	10.9	7	0.06±0.01	10
IBH	0.5±0.11	0.8±0.15	13.6	7.6	0.14±0.04	11.5
ISH	0.4±0.08	0.7±0.14	7.9	5.9	0.13±0.04	13
ThT	0.04±0.01	7.6±2.1	2.8	1.2	0.03±0.01	[d] –

[a] Parameters given for A4, A6, A8, AM1, AM2, AM3 and AM4 have been reported in our previous work [20], but the Q values of these dyes were corrected to the refractive indexes of amyloid fibrils and ethanol, and the Q value of Rhodamine 101 was assumed to be 0.91

[b] The dyes A6, A8 and AM1 showed no changes in their fluorescence intensities upon addition of monomeric lysozyme, therefore I/I_{nat} was not calculated for these dyes

[c] REES was measured with increasing wavelength from 430 nm to 450 nm for all dyes

[d] REES was not measured for Thioflavin T

slows down protein diffusion and serves as the positive effector of intermolecular β-sheet formation [36]. This conformation is characterized by the expanded α-helical content, disturbed hydration shell and tertiary structure dictated by protein interactions with the organic solvent [36, 37]. Specifically, lower dielectric constant of the protein environment gives rise to decrease in protein hydration, which, in turn, reduces inter- and intramolecular hydrophobic interactions and induces solvent exposure of hydrophobic patches. This was demonstrated, for instance, for LYS (11–36) peptide in trifluoroethanol [38]. Likewise, ethanol enhances intra- and intermolecular H-bonds compared to their strength in aqueous environment [39]. In the presence of ethanol solvent ability to compete with peptide carbonyl acceptor significantly decreases [38]. Importantly, it was demonstrated that ethanol alone produces only insignificant partial unfolding of HEWL, and agitation enhances monomer probability to encounter a hydrophobic surface leading to protein destabilization [22, 29].

In turn, low pH (~ 2) and the midpoint temperature for HEWL unfolding (57 °C) [40] were found to be the most

Table 3 Binding characteristics of benzanthrone dyes associated with lysozyme fibrils prepared by acidic denaturation (F_{ac})

Dye	K_a, μM^{-1}	n	I/I_0	I/I_{nat}	Q	[b] REES, nm
A4	0.06±0.01	1±0.2	1.2	1.2	0.02±0.004	8
A6	1.2±0.02	0.22±0.04	1.5	[a] –	0.31±0.07	16
A8	0.82±0.18	0.04±0.01	1.1	[a] –	0.65±0.14	22
AM1	2.1±0.4	0.13±0.03	3.5	[a] –	0.08±0.016	10
AM2	0.06±0.02	0.8±0.16	1.7	0.14	0.04±0.01	22
AM3	0.29±0.06	0.43±0.09	2.7	0.6	0.10±0.022	30
AM4	0.1±0.02	1.7±0.3	2.5	1.9	0.27±0.06	17
AM12	0.7±0.14	0.21±0.05	1.8	4.2	0.20±0.05	18
AM15	0.23±0.05	0.08±0.02	1.8	2.7	0.42±0.09	17
AM18	4.6±0.9	0.54±0.12	6.5	0.5	0.26±0.06	17
IAH	2.3±0.5	0.21±0.04	6.1	4.3	0.11±0.023	14
IBH	0.15±0.03	0.7±0.015	2.3	1.4	0.11±0.022	15
ISH	0.08±0.02	3.9±0.08	6.4	3.5	0.30±0.06	12
ThT	0.03±0.005	2±0.3	1.4	0.7	0.01±0.002	[c] –

[a] The dyes A6, A8 and AM1 showed no changes in their fluorescence intensities upon addition of monomeric lysozyme, therefore I/I_{nat} was not calculated for these dyes

[b] REES was measured with increasing wavelength from 500 nm to 570 nm for A4, IAH, IBH, ISH, and from 470 nm to 540 nm for the rest of the dyes

[c] REES was not measured for Thioflavin T

Fig. 4 TEM images of lysozyme fibrils prepared in concentrated ethanol solution – F_{eth} (**a**) or by acidic denaturation – F_{ac} (**b**). Scale bars represent 200 and 100 nm, respectively
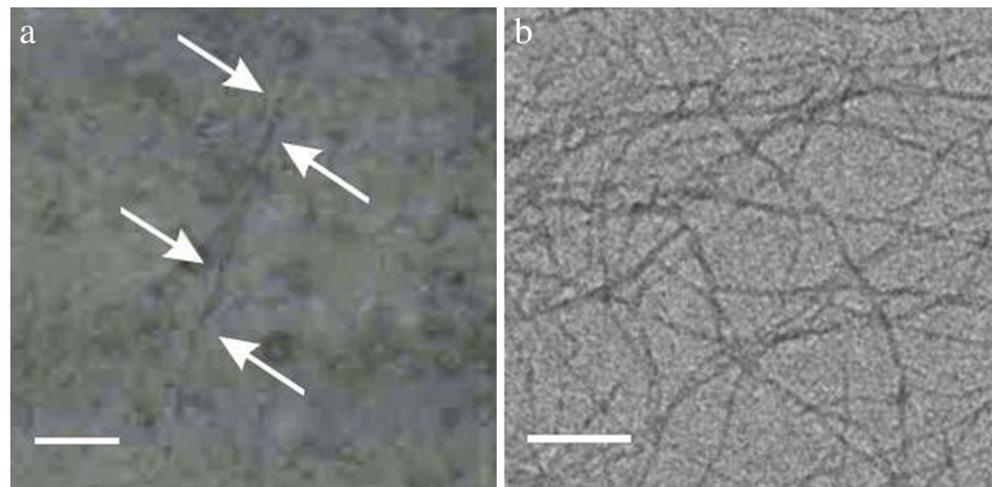
favorable for amyloid formation [39, 40]. Partially unfolded protein state formed under these conditions is characterized by substantial loss of tertiary and partial loss of secondary structure [31, 39]. The changes in lysozyme conformation are controlled by several factors. First, the neutrality of glutamic and aspartic acid residues at pH 2 leads to increase of the protein positive charge and enhances intermolecular charge repulsion [41, 42]. Furthermore, both pH 2 [23, 39] and elevated temperature [43] cause partial exposure of protein hydrophobic patches to the solvent and weaken intramolecular hydrogen bonding [44, 45]. Next, acidic pH [46] and high temperature [47] presumably induce a decrease of lysozyme hydration. Finally, lysozyme incubation under these conditions may lead to more profound changes in the protein secondary structure compared to those induced by its agitation in the presence of ethanol at neutral pH [22, 29]. Interestingly, very stable HEWL molecule adopts native conformation even at pH ~ 0.6 [48], but only combination of low pH and high temperature promotes protein fibrillogenesis. This indicates that enhanced a fragmentation was observed upon its prolonged incubation at acidic pH and elevated temperature [23, 32], raising the possibility for protein fragments to be included into fibril structure.

Schematic representation of the above two HEWL partially unfolded states is given in Fig. 5. Altogether, lysozyme, partially unfolded the presence of 80 % ethanol at pH 7.4, is characterized by the enhanced solvent exposure of hydrophobic patches [38], reduced hydration [35] and increased inter- and intramolecular H-bonding [39]. In turn, at pH 2 and 60 °C lysozyme possesses partially solvent-exposed hydrophobic areas [23, 43] along with higher net positive charge [42]. Furthermore, similar to other proteins, lysozyme subjected to low pH and elevated temperature, is likely to have reduced intramolecular H-bonding [44, 45] and hydration [46, 47]. In general, the F_{eth}-forming monomers are presumably less destabilized compared to the F_{ac}-forming monomers, thereby accounting for the lower rate of fibril growth in the presence of

80 % EtOH at neutral pH [22, 49]. Notably, hydrophobic interactions and electrostatic repulsion between side chains seem to play more important role in F_{ac} fibrillogenesis, compared to F_{eth}. The above structural peculiarities of lysozyme partially unfolded states may account for morphological differences of F_{eth} and F_{ac} fibrils. These differences may include: i) distinct protofilament number; ii) particular protofilament arrangement; iii) distinct "steric zipper" structures [50]. For instance, Zurdo and coworkers have established pH dependency of protofilament number and packing in fibrillar SH3-domain, that was interpreted in terms of the variations in electrostatic interactions between protein molecules [41]. Verel and coauthors observed different stacking of the two β-sheets in a "steric zipper" of fibrils formed from the model peptide ccβ-p at acidic and neutral pH [51]. Petkova et al. found that the β-sheets of Aβ (11–25) at acidic pH are composed of shorter β-strands than at neutral pH [52].

Finally, greater diameter of F_{eth} compared to F_{ac} can result from the higher thickness and number of protofilaments assembled into fibril structure [2, 4]. The latter is presumably caused by the agitation-enhanced association of protofilaments [53] and electrostatic stabilization of the final
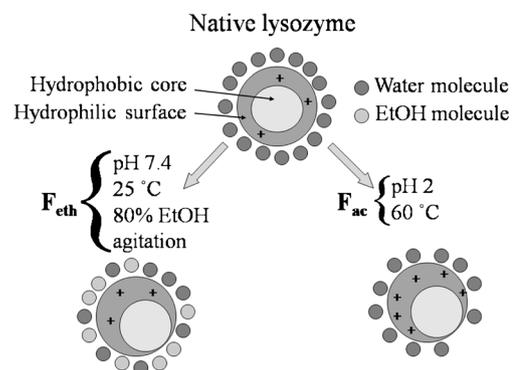
Fig. 5 Schematic representation of the partially unfolded lysozyme states under two different conditions resulting in the formation of F_{eth} or F_{ac} fibrils

complex [54]. Interestingly, stronger lateral association of protofilaments may lead to a decrease in fibril elongation [55, 56]. This may be the reason for the observed slightly lower length of F_{eth} compared to F_{ac}.

Benzanthrone Amyloid Specificity Ranking

At the next step of the study the recovered binding parameters, K_a, n and α were used to calculate two additional quantities characterizing the dye fibril specificity: i) I/I_0 —relative fluorescence intensity increase upon the dye (1 μM) binding to fibrillar lysozyme (2 μM); ii) I/I_{nat}—binding preference of the dye (1 μM) to fibrillar aggregates (2 μM) (Tables 2 and 3). This allowed us to range benzanthrones according to their specificity either to F_{eth} or F_{ac} (Table 4). It appeared that among F_{eth}-bound dyes AM2 showed the highest I/I_0 (ca. 38) and Q (ca. 0.77) coupled with high I/I_{nat} (ca. 5). At the same time, AM2 displayed the greatest sensitivity to fibril morphology, as judged from the drastic difference between Q values in F_{eth} (ca. 0.77) and F_{ac} (ca. 0.04) systems. The dyes A6 and A8 appeared to be suitable for highly sensitive detection of amyloid fibrils of both F_{eth} and F_{ac} types. It should also be noted that all other benzanthrones with quantum yields differing in F_{eth}- and F_{ac}-bound states can also be used for conformational typing of amyloid structures. Importantly, all novel dyes displayed much higher sensitivity to lysozyme fibrils than classical amyloid marker ThT, as judged from the comparison of I/I_0, I/I_{nat}, Q and K_a values.

Characterization of Fibril Binding Sites for Benzanthrone Dyes

Next, to explain the differences in BD association with F_{eth} and F_{ac} and their higher amyloid sensitivity compared to ThT, it was of interest to define putative dye-fibril binding sites. Several lines of evidence indicate that classical amyloid dyes ThT and Congo Red (CR) predominantly occupy the channels between the side chains, being the common motif in cross-β structure and running parallel to fibril axis [57, 58]. These sites proved to account for characteristic ThT fluorescence and CR birefringence, in contrast to alternative sites, viz. hydrophobic cavities [59], dry "steric zipper" interface [60], β-sheet surface [60] and β-sheet edges [61]. Thus, it cannot be excluded that considerable increase in benzanthrone quantum yield results from the dye association with fibril grooves. This assumption is further confirmed by close dimensions of BD and classical amyloid reporters. Specifically, BD are ~1.1–2 nm in length,

~0.7–1 nm in width and ~0.3–0.8 nm in thickness, while analogous dimensions of ThT are 1.5, 0.6 and 0.4 nm, respectively [62]. Therefore, we can suppose that BD, similar to ThT and CR, associate with the channels formed by side chain rows consisting of 4–5 amino acid residues and running in the direction of β-sheet propagation [57, 62].

In our recent work red edge excitation shift (REES) approach was used to define BD binding sites in F_{eth} fibrils [20]. REES is a red shift in the dye emission maxima induced by the shift in excitation wavelength toward the red edge of the absorption band. REES arises from the slowed rates of solvent relaxation around the excited state fluorophore which reflects the motional restrictions imposed on the solvent molecule in the immediate vicinity of the dye [9, 63]. In the case of protein-bound dyes the presence of REES indicates the restricted mobility of both the protein polar groups and the protein-bound water molecules on nanosecond scale (i.e. during the excited state lifetime) [64]. In the present study we measured REES for F_{eth}-bound AM12, AM15, AM18, IAH, IBH and ISH and made an attempt to localize their binding sites. REES value for each dye was calculated as the difference between emission maxima of the probe excited at 450 and 430 nm (Table 2). We also extended our investigation to the F_{ac}-bound fluorophores by measuring their REES values as the difference between emission maxima of the probe excited at: i) 500 and 570 nm (for A4, IAH, IBH and ISH); ii) 470 and 540 nm (for the rest of 13 dyes) (Table 3). These wavelength ranges are wider (70 nm) compared to the above ones (20 nm) and seem to give more precise results. Since the REES of F_{eth}- and F_{ac}-bound probes were taken within different wavelength ranges, comparison of the REES values for the dyes bound to different types of lysozyme fibrils appeared to be problematic, but we compared the REES values of the different dyes associated either with F_{eth}- or F_{ac}. The representative spectra of BD with the excitation wavelength dependent emission maxima are given in Fig. 6. The existence of red shifts in BD emission maxima, following red shift in excitation wavelength, indicates the presence of restricted solvent in close vicinity of the dye [9, 65]. Taking into consideration that the wet "steric zipper" interface is characterized by the presence of high amount of polar residues lined with water molecules [66] with every polar residue being hydrated, it can be supposed that BD associate presumably with the surface grooves of amyloid fibrils. The observed differences in REES values may occur from distinct photophysical changes upon excitation induced by distinct structures of 3-aminosubstituents of the benzanthrone moiety.

Table 4 Dye rows showing the decrease of benzanthrone sensitivity to lysozyme fibrils prepared under different conditions

| F_{eth} | AM2 | AM1 | A8 | A6 | IBH | AM3 | AM4 | AM18 | IAH | ISH | AM15 | AM12 | A4 | ThT |
| F_{ac} | A8 | A6 | ISH | AM18 | IAH | AM1 | AM15 | AM12 | AM4 | IBH | AM3 | AM2 | A4 | ThT |
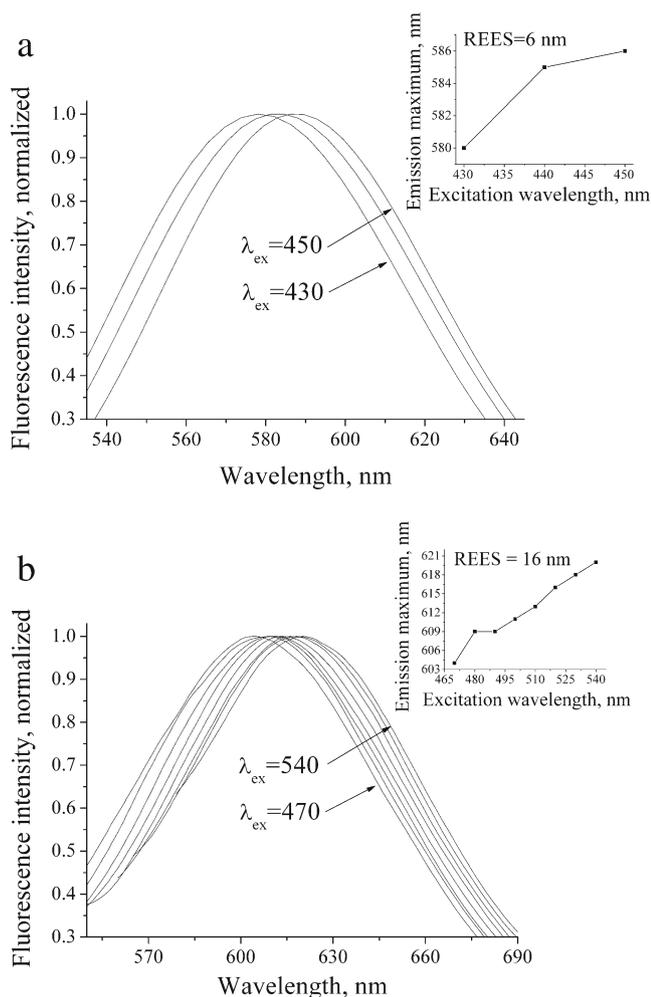
Fig. 6 Fluorescence spectra of A6 bound to F_{ac} at increasing excitation wavelength (**a**) and red edge excitation shift (REES) of the dye emission maximum (**b**). A6 and F_{ac} concentrations were 0.65 and 30 μM, respectively

Notably, we failed to detect REES for AM12, AM15 and AM18 in the presence of F_{eth}. These dyes seem to reside at the dry "steric zipper" interface [57, 67], similar to other benzanthrone amino derivatives AM2 and AM3 [20]. The dry "steric zipper" interface is characterized by a large number of hydrophobic amino acids and the absence of water molecules, leading to disappearance of the dye-water dipole-dipole interactions, compared to wet "steric zipper" interface [68]. This may lead to REES weakening or even its elimination. Interestingly, high REES values were observed for the remaining BD belonging predominantly to the family of benzanthrone amidino derivatives (except of AM1 and AM4). Presumably, association of the dyes with the dry "steric zipper" interface is hampered because of strong complementarity between stacking β-sheets, resulting in highly limited space for fluorophore insertion (Table 2) [57]. Of value in this regard may be also the dye hydrophobicity.

In turn, all BD showed high REES values in the presence of F_{ac} (Table 3) close to the values for the rest of F_{ac}-incorporated fluorophores. Therefore, these probes are likely to occupy the wet "steric zipper" interface of amyloid fibrils. This may arise from the tighter packing of β-sheets in a "steric zipper" of F_{ac}, hampering the dye penetration into the dry "steric zipper" interface as was observed for the F_{eth}-bound dyes. In the case of AM2 and AM3 the transition of the dye-protein binding site from the dry to wet "steric zipper" interface may explain high sensitivity of these fluorophores to fibril morphology, leading to large differences in the quantum yields of F_{eth}- and F_{ac}-bound probes.

To better understand the REES data, at the next step of the study we performed time-resolved fluorescence measurements. The fluorescence lifetimes of the dyes were determined in the presence of F_{ac} (dye-protein ratio was varied from 1:4 to 1:25 for the different dyes). For the sake of comparison, we also measured time-resolved fluorescence intensity decays of BD in DMF. The representative time-resolved fluorescence intensity decays of BD in DMF and in the presence of F_{ac} are given in Fig. 7. The BD decays in DMF were fitted to mono-exponential decay (Eq. 2), by analogy with the other members of the benzanthrone family, i.e. metoxybenzanthrone (MBA) [69]. Furthermore, the logarithmic intensity vs time plots turned out to be linear, confirming that BD fluorescence in DMF do show the mono-exponential decay [9]. Interestingly, the calculated lifetime values for BD in DMF were close to the MBA fluorescence lifetime (*ca.* 12 ns) [67].

Next, we fitted the fluorescence lifetime decay of BD in the presence of F_{ac} by biexponential function. It was supposed that the longer lifetime component (τ_1) corresponds to the lifetime of the amyloid-bound dye (lower environmental polarity compared to buffer solution), while the shorter component accounts for the free dye in buffer (polar environment), as was observed e.g. for amyloid markers Nile Red and ANS [70, 71]. Indeed, we found that τ_1 values in the presence of F_{ac} were close to those in DMF (Table 5). From these data we concluded that environmental polarity of the amyloid-bound dye is lower compared to buffer solution and close to that of DMF ($\varepsilon_{DMF} \approx 37$). On the other side, fluorescence lifetime may also increase with the solvent viscosity, as has been demonstrated e.g. for Thioflavin T [72]. The shorter lifetime component τ_2 presumably corresponds to fluorescence lifetime of the dye molecules in a buffer solution (Table 5).

The fact that all BD demonstrated REES in the presence of F_{ac} is suggestive of the "rigidity" of their environment, hampering the separation of polarity and viscosity effects on the value of longer lifetime component τ_1. Furthermore, τ_1, its fractional contribution f_1 (calculated from Eq. 3) to the steady-state intensity, and the average lifetime $<\tau>$ (calculated from Eq. 4) were proportional to the REES values of these probes (except of A4, AM1, AM2, AM3) (Table 3). These data can be interpreted as follows: although all dyes presumably
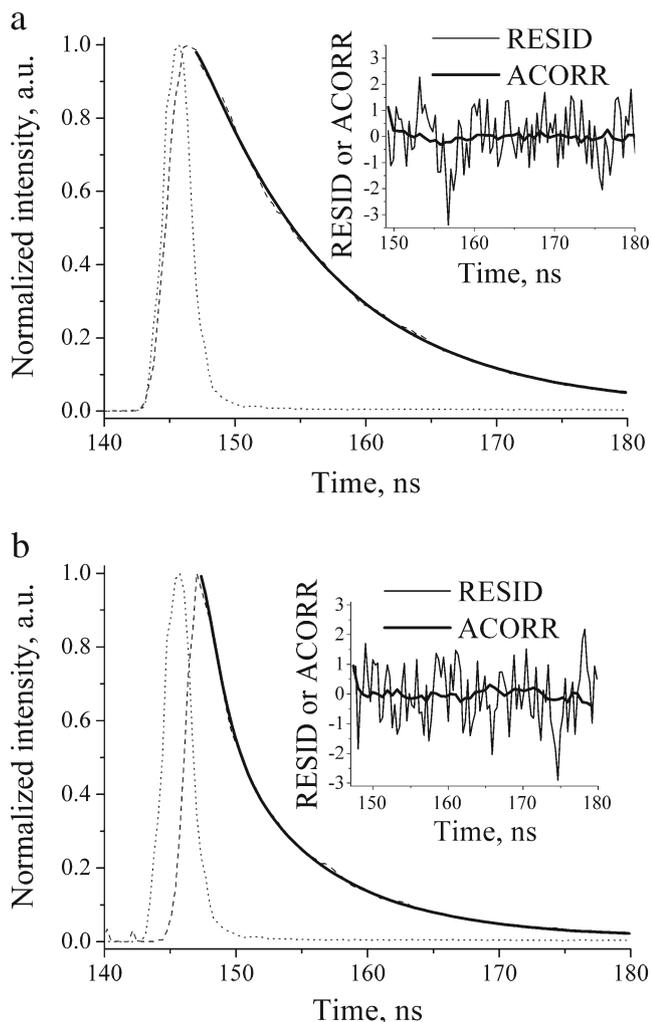
Fig. 7 Time-resolved fluorescence intensity decay of AM12 in dimethylformamide (**a**), and of F_{ac}-bound AM12 (**b**). Decay profiles (dashed lines) were fitted to mono- (**a**) and bi-exponential (**b**) functions (solid lines). Dye was excited at 421 nm and emission was monitored at 585 nm. Lamp profile (dotted lines) was measured at the excitation wavelength using Ludox as the scatterer. AM12 concentration was 0.4 μM. The insets show the weighted residuals and the autocorrelation function of the weighted residuals

occupy one type of binding sites – fibril grooves, local solvent relaxation times may vary depending on the mobility of the amino acid residues of the protein binding site for each dye. Therefore, increase of τ_1 (as well as f_1, and $<\tau>$ as a consequence) proportionally to the REES may indicate the increase of the local rigidity of the environment of BD (Tables 3 and 5). Fibril-associating properties of A4, AM1, AM2 and AM3 seem to be different compared to the other dyes, as judged from their low quantum yields in the presence of F_{ac} and the absence of correlation between the fluorescence lifetimes and REES.

By and large, time-resolved fluorescence measurements of BD in DMF and in the presence of F_{ac} showed that these dyes

are associated with one type of the fibril binding sites characterized by lower polarity compared to buffer solution. These results corroborate the notion that high REES values acquired from the steady-state measurements, reflect rather high viscosity of the above binding site represented by the fibril grooves. Furthermore, the proportionality of the fluorescence lifetimes of BD to the REES values indicate that the novel dyes similar to ThT, have the sensitivity of the lifetimes to the solvent viscosity [72]. Although we did not perform the lifetime measurements of the dyes incorporated into F_{eth}, it can be supposed that they also have one fluorescence lifetime component corresponding to the lifetime of dye molecules incorporated into the fibril grooves (because they show high REES values as well). Finally, the assumption that the dyes AM2, AM3, AM12, AM15 and AM18 can be embedded into fibril dry "steric zipper" can be also tested by the fluorescence lifetime measurements of the F_{eth}-incorporated dyes.

Comparison of Amyloid Specificity of Benzanthrone Dyes and Thioflavin T

Assuming that fibril grooves are the common binding sites for BD and ThT, we tried to determine the differences in the interactions of the dyes with amyloid fibrils, leading to their distinct amyloid sensitivity (Tables 2 and 3). In this regard, it is important to analyse what kinds of interactions may occur between small organic molecules and fibrillar aggregates. Classical amyloid markers ThT and CR specifically associate with the surface aromatic grooves, presenting large hydrophobic areas to interact with small ligands and thus allowing their insertion into fibril structure [57, 73]. Additionally, van der Waals contacts seem to occur between the dyes and backbone of the groove-forming residues [73, 74]. Furthermore, steric and aromatic interactions [49, 75] may play essential role in determining the binding preference of the dyes. Finally, electrostatic interactions are important for ThT and CR association with amyloid fibrils. For example, ThT does not bind to positively charged poly-L-lysine [76] and has low binding capability to HET-s prion (218–289) fibrils at acidic pH compared to neutral pH [77]. It was demonstrated that salt bridges between two sulfonic groups of CR and positively charged amino acid residues are required for the dye association with poly-L-lysine, HET-s prion (218–289), Aβ (1–42) fibrillar aggregates, etc. [58, 61, 78].

The above data allowed us to make the assumption, why the majority of F_{eth} and F_{ac}-bound BD have 1–2 order of magnitude higher association constants and quantum yields compared to ThT (Tables 2 and 3). These differences can arise predominantly from higher hydrophobicity of BD originating from the absence of charged groups and the presence of aromatic benzanthrone moiety. In view of this, BD similar to the neutral ThT derivative, Pittsburgh compound B, may show deeper insertion into fibril grooves compared to ThT,

Table 5 Fluorescence lifetimes of benzanthrone dyes excited at 421 nm in dimethylformamide (DMF) and in the presence of lysozyme fibrils prepared by acidic denaturation (F_{ac})

Dye	DMF		F_{ac}					
	$^{a}\tau$, ns	$^{b}\chi^2$	$^{c}\tau_1$, ns	$^{c}\tau_2$, ns	$^{d}f_1$	$^{d}f_2$	$^{c}\langle\tau\rangle$, ns	$^{b}\chi^2$
A4	8.2±0.4	1.02	6.7±0.42	1.6±0.16	0.41	0.59	3.7	0.97
A6	9.8±0.05	1.04	7.8±0.21	1.3±0.25	0.75	0.25	6.1	1.02
A8	5.8±0.01	1.01	8.3±0.24	1.3±0.11	0.51	0.48	4.9	0.98
AM1	3.9±0.2	1.16	7.5±0.03	1.59±0.002	0.61	0.39	5.2	1.11
AM2	8.2±0.04	1.08	7.1±0.16	0.73±0.06	0.31	0.69	2.7	1.01
AM3	8.6±0.05	1.02	5.6±0.64	0.55±0.08	0.45	0.55	2.8	1.05
AM4	8.5±0.05	0.87	8.1±0.37	2.00±0.2	0.55	0.45	5.3	1.02
AM12	8.7±0.005	0.94	6.8±0.25	1.55±0.24	0.69	0.31	5.2	0.83
AM15	8.3±0.03	0.89	6.7±0.08	0.72±0.09	0.59	0.41	4.24	1.01
AM18	7.5±0.04	1.09	6.8±0.19	2.09±0.14	0.45	0.55	4.23	1.08
IAH	6.8±0.15	0.98	6.0±0.35	1.32±0.3	0.43	0.57	3.33	0.88
IBH	8.3±0.08	0.95	6.2±0.16	0.46±0.17	0.54	0.46	3.6	0.95
ISH	7.5±0.01	1.30	5.9±0.35	1.14±0.11	0.32	0.67	2.7	1.05

[a] Fluorescence lifetime of AM12 in DMF

[b] The reduced chi-square values characterizing the goodness of the fits of the experimental decay profiles

[c] Fluorescence lifetime components of AM12 in the presence of F_{ac}

[d] Fractional contributions of the each decay time to the steady-state intensity of the dyes in the presence of F_{ac}

leading to the enhancement of dye-protein aromatic, steric and hydrophobic interactions [74]. Furthermore, high hydrophobicity of BD creates prerequisites for their association with the hydrophobic dry "steric zipper" interface, as was supposed for AM2, AM3, AM12, AM15 and AM18 (Table 2).

Distinct Morphologies of Lysozyme Amyloid Fibrils Probed by Benzanthrones

Finally, based on the foresaid structural differences between F_{eth} and F_{ac}, as well as on the assumption that BD tend to localize in the surface grooves or at the dry "steric zipper" interface of amyloid fibrils, we made an attempt to explain distinct spectral properties of the F_{eth}- and F_{ac}-incorporated dyes (Tables 1, 2 and 3). First, we analyzed ThT sensitivity to amyloid morphology and then drew an analogy with BD. Obviously, the reduced binding stoichiometry and the lower quantum yield of F_{ac}-incorporated ThT compared to the corresponding parameters of F_{eth}-bound dye result from the difference in the arrangement of β-strands in β-sheets formed at acidic and neutral pH [51, 52]. Specifically, F_{ac} protofilaments formed at acidic pH are presumably composed of shorter β-strands than those of F_{eth} formed at neutral pH, similar to the protofilaments of fibrillar Aβ (11–25) [52]. This can reduce the total number of grooves in amyloid fibrils and can lead to the decrease of ThT binding stoichiometry. Furthermore, F_{eth} and F_{ac} are presumably made of β-sheets with distinct hydrophobic clustering, similarly to amyloid fibrils of the model peptide ccβ-p formed at neutral or low pH [51]. More specifically, Verel and coworkers have found two kinds of grooves in the β-sheet of model peptide ccβ-p at neutral pH: i) the grooves formed solely from the uncharged amino acid residues, undergoing a hydrophobic clustering; ii) the channels lined with the charged residues, where the charge

compensation between positively and negatively charged residues takes place [51]. In turn, at acidic pH the protonation of Glu side chains may disturb hydrophobic clustering of amino acid residues [51]. This effect, being extrapolated to HEWL fibrils formed at acidic pH could result in a larger number of the grooves containing positively charged Arg residues, thereby hampering ThT insertion.

By analogy with ThT, lower association constants of about a half of F_{ac}-bound BD compared to F_{eth}, can be explained by their unfavorable interactions with the increased number of the charged fibril grooves. In this respect, BD resemble the neutral ThT derivative, Pittsburgh compound B, which does not favor binding to the charged fibril grooves, as well [74]. In turn, lower F_{ac} binding stoichiometries of the majority of the probes seem to be related to the lower number of the surface grooves in F_{ac} core structure. Furthermore, it cannot be excluded that F_{ac} protofilaments are packed more tightly than F_{eth} protofilaments. This may result in the smaller size of fibril grooves hampering deep BD penetration into fibril interior. Accordingly, increased microenvironmental polarity may induce red shift of the emission maxima of the majority of F_{ac}-incorporated BD and ThT (Table 1). As a consequence, quantum yield of eight F_{ac}-incorporated BD appears to be lower than that of F_{eth}-bound dyes. However, the observed ambiguous changes of BD quantum yield in the presence of F_{ac} indicate that not only fibril morphology, but also subtle chemical structure of these fluorophores may play essential role in the dye complexation with fibrillar protein.

Conclusions

In conclusion, the present study has been undertaken to evaluate the potential of the novel benzanthrone dyes to

selectively detect lysozyme fibrillar aggregates with different morphologies. Based on the comprehensive analysis of spectral characteristics of a series of benzanthrones bound to amyloid fibrils obtained by ethanol and acid denaturation, we recommend AM2 as the best candidate for identifying the differences in fibril architecture, while structurally-insensitive amyloid tracers A8 and A6 can be employed as alternative to ThT. A detailed comparative analysis of BD and ThT interactions with amyloid fibrils may prove of importance in the design of effective anti-amyloid drugs.

References

1. Uversky VN, Fink AL (2004) Conformational constraints for amyloid fibrillation: the importance of being unfolded. Biochim Biophys Acta 1698:131–153
2. Hill SE, Miti T, Richmond T, Muschol M (2011) Spatial extent of charge repulsion regulates assembly pathways for lysozyme amyloid fibrils. PLoS ONE 6:e18171
3. Meijer JT, Roeters M, Viola V, Löwik DW, Vriend G, van Hest JC (2007) Stabilization of peptide fibrils by hydrophobic interaction. Langmuir 23:2058–2063
4. Chamberlain AK, MacPhee CE, Zurdo J, Morozova-Roche LA, Hill HA, Dobson CM, Davis JJ (2000) Ultrastructural organization of amyloid fibrils by atomic force microscopy. Biophys J 79:3282–3293
5. Gharibyan AL, Zamotin V, Yanamandra K, Moskaleva OS, Margulis BA, Kostanyan IA, Morozova-Roche LA (2007) Lysozyme amyloid oligomers and fibrils induce cellular death via different apoptotic/necrotic pathways. J Mol Biol 365:1337–1349
6. Wigenius J, Persson G, Widengren J, Inganäs O (2011) Interactions between a luminescent conjugated oligoelectrolyte and insulin during early phase of amyloid formation. Macromol Biosci 11:1120–1127
7. Dusa A, Kaylor J, Edridge S, Bodner N, Hong DP, Fink AL (2006) Characterization of oligomers during alpha-synuclein aggregation using intrinsic tryptophan fluorescence. Biochemistry 45:2752–2760
8. Gorbenko GP (2011) Fluorescence spectroscopy of protein oligomerization in membranes. J Fluoresc 21:945–951
9. Lakowicz JR (2006) Principles of fluorescence spectroscopy, 3rd edn. Springer, New York
10. Qin L, Vastl J, Gao J (2010) Highly sensitive amyloid detection enabled by thioflavin T dimers. Mol Biosyst 6:1791–1795
11. Naiki H, Higuchi K, Hosokawa M, Takeda T (1989) Fluorometric determination of amyloid fibrils in vitro using the fluorescent dye, thioflavine T. Anal Biochem 177:244–249
12. Bertoncini CW, Celej MS (2011) Small molecule fluorescent probes for the detection of amyloid self-assembly in vitro and in vivo. Curr Protein Pept Sci 12:205–220
13. Celej MS, Jares-Erijman EA, Jovin TM (2008) Fluorescent N-arylaminonaphthalene sulfonate probes for amyloid aggregation of alpha-synuclein. Biophys J 94:4867–4879
14. Mishra R, Sjölander D, Hammarström P (2011) Spectroscopic characterization of diverse amyloid fibrils in vitro by the fluorescent dye Nile red. Mol Biosyst 7:1232–1240
15. Makwana PK, Jethva PN, Roy I (2011) Coumarin 6 and 1,6-diphenyl-1,3,5-hexatriene (DPH) as fluorescent probes to monitor protein aggregation. Analyst 136:2161–2167
16. Ribeiro MG, Vicente MH, Santos IC, Santos I, Outeiro TF, Paulo A (2011) Synthesis and in vitro evaluation of fluorinated styryl benzazoles as amyloid-probes. Bioorg Med Chem 19:7698–7710
17. Ran C, Xu X, Raymond SB, Ferrara BJ, Neal K, Bacskai BJ, Medarova Z, Moore A (2009) Design, synthesis, and testing of difluoroboron derivatized curcumins as near infrared probes for in vivo detection of amyloid-β deposits. J Am Chem Soc 131:15257–15261
18. Kundu B, Guptasarma P (2002) Use of a hydrophobic dye to indirectly probe the structural organization and conformational plasticity of molecules in amorphous aggregates of carbonic anhydrase. Biochem Biophys Res Commun 293:572–577
19. Sabaté R, Lascu I, Saupe SJ (2008) On the binding of Thioflavin-T to HET-s amyloid fibrils assembled at pH 2. J Struct Biol 162:387–396
20. Vus K, Trusova V, Gorbenko G, Kirilova E, Kirilov G, Kalnina I, Kinnunen P (2012) Novel aminobenzanthrone dyes for amyloid fibril detection. Chem Phys Lett 532:110–115
21. Kirilova EM, Kalnina I, Kirilov GK, Meirovics I (2008) Spectroscopic study of benzanthrone 3-N-derivatives as new hydrophobic fluorescent probes for biomolecules. J Fluoresc 18:645–648
22. Holley M, Eginton C, Schaefer D, Brown LR (2008) Characterization of amyloidogenesis of hen egg lysozyme in concentrated ethanol solution. Biochem Biophys Res Commun 373:164–168
23. Morozova-Roche LA, Zurdo J, Spencer A, Noppe W, Receveur V, Archer DB, Joniau M, Dobson CM (2000) Amyloid fibril formation and seeding by wild-type human lysozyme and its disease-related mutational variants. J Struct Biol 130:339–351
24. Rurack K, Spieles M (2011) Fluorescence quantum yields of a series of red and near-infrared dyes emitting at 600–1000 nm. Anal Chem 83:1232–1242
25. Appel TR, Richter S, Linke RP, Makovitzky J (2005) Histochemical and topo-optical investigations on tissue-isolated and in vitro amyloid fibrils. Amyloid 12:174–183
26. Dienes A (1975) Comparative gain measurements for twelve organic laser dye solutions. J Appl Phys 7:135–139
27. Chattopadhyay A, Mukherjee S (1999) Depth-dependent solvent relaxation in membranes: wavelength-selective fluorescence as a membrane dipstick. Langmuir 15:2142–2148
28. Lindgren M, Sörgjerd K, Hammarström P (2005) Detection and characterization of aggregates, prefibrillar amyloidogenic oligomers, and protofibrils using fluorescence spectroscopy. Biophys J 88:4200–4212
29. Sasahara K, Yagi H, Sakai M, Naiki H, Goto Y (2008) Amyloid nucleation triggered by agitation of β2-microglobulin under acidic and neutral pH conditions. Biochemistry 47:2650–2660
30. Morel B, Varela L, Azuaga AI, Conejero-Lara F (2010) Environmental conditions affect the kinetics of nucleation of amyloid fibrils and determine their morphology. Biophys J 99:3801–3810
31. Morozova-Roche LA (2007) Equine lysozyme: the molecular basis of folding, self-assembly and innate amyloid toxicity. FEBS Lett 581:2587–2592
32. Frare E, Polverino De Laureto P, Zurdo J, Dobson CM, Fontana A (2004) A highly amyloidogenic region of hen lysozyme. J Mol Biol 340:1153–1165
33. Malisauskas M, Zamotin V, Jass J, Noppe W, Dobson CM, Morozova-Roche LA (2003) Amyloid protofilaments from the calcium-binding protein equine lysozyme: formation of ring and linear structures depends on pH and metal ion concentration. J Mol Biol 330:879–890
34. Goda S, Takano K, Yamagata Y, Nagata R, Akutsu H, Maki S, Namba K, Yutani K (2000) Amyloid protofilament formation of hen egg lysozyme in highly concentrated ethanol solution. Protein Sci 9:369–375
35. Yonezawa Y, Tanaka S, Kubota T, Wakabayashi K, Yutani K, Fujiwara S (2002) An insight into the pathway of the amyloid fibril formation of hen egg white lysozyme obtained from a small-angle X-ray and neutron scattering study. J Mol Biol 323:237–351
36. Tanaka S, Oda Y, Ataka M, Onuma K, Fujiwara S, Yonezawa Y (2001) Denaturation and aggregation of hen egg lysozyme in aqueous ethanol solution studied by dynamic light scattering. Biopolymers 59:370–379

37. Lehmann MS, Mason SA, McIntyre GJ (1985) Study of ethanol-lysozyme interactions using neutron diffraction. Biochemistry 24:5862–5869

38. Liu W, Prausnitz JM, Blanch HW (2004) Amyloid fibril formation by peptide LYS (11–36) in aqueous trifluoroethanol. Biomacromolecules 5:1818–1823

39. Aso Y, Shiraki K, Takagi M (2007) Systematic analysis of aggregates from 38 kinds of non disease-related proteins: identifying the intrinsic propensity of polypeptides to form amyloid fibrils. Biosci Biotechnol Biochem 71:1313–1321

40. Arnaudov LN, de Vries R (2005) Thermally induced fibrillar aggregation of hen egg white lysozyme. Biophys J 88:515–526

41. Zurdo J, Guijarro JI, Jiménez JL, Saibil HR, Dobson CM (2001) Dependence on solution conditions of aggregation and amyloid formation by an SH3 domain. J Mol Biol 311:325–340

42. Kuehner DE, Engmann J, Fergg F, Wernick M, Blanch HW, Prausnitz JM (1999) Lysozyme net charge and ion binding in concentrated aqueous electrolyte solutions. J Phys Chem B 103:1368–1374

43. Tani F, Murata M, Higasa T, Goto M, Kitabatake N, Doi E (1995) Molten globule state of protein molecules in heat-induced transparent food gels. J Agric Food Chem 43:2325–2331

44. Tomlinson JH, Craven CJ, Williamson MP, Pandya MJ (2009) Dimerization of protein G B1 domain at low pH: a conformational switch caused by loss of a single hydrogen bond. Proteins 78:1652–1661

45. Cordier F, Grzesiek S (2002) Temperature-dependence of protein hydrogen bond properties as studied by high-resolution NMR. J Mol Biol 317:739–752

46. Durchschlag H, Zipper P (2004) Modeling the hydration of proteins at different pH values. Progr Colloid Polym Sci 127:98–112

47. Zhang Y, Lagi M, Liu D, Mallamace F, Fratini E, Baglioni P, Mamontov E, Hagen M, Chen SH (2009) Observation of high-temperature dynamic crossover in protein hydration water and its relation to reversible denaturation of lysozyme. J Chem Phys 130:135101

48. Sasahara K, Demura M, Nitta K (2000) Partially unfolded equilibrium state of hen lysozyme studied by circular dichroism spectroscopy. Biochemistry 39:6475–6482

49. Krebs MR, Wilkins DK, Chung EW, Pitkeathly MC, Chamberlain AK, Zurdo J, Robinson CV, Dobson CM (2000) Formation and seeding of amyloid fibrils from wild-type hen lysozyme and a peptide fragment from the beta-domain. J Mol Biol 300:541–549

50. Fändrich M, Meinhardt J, Grigorieff N (2009) Structural polymorphism of Alzheimer Abeta and other amyloid fibrils. Prion 3:89–93

51. Verel R, Tomka IT, Bertozzi C, Cadalbert R, Kammerer RA, Steinmetz MO, Meier BH (2008) Polymorphism in an amyloid-like fibril-forming model peptide. Angew Chem Int Ed Engl 47:5842–5845

52. Petkova AT, Buntkowsky G, Dyda F, Leapman RD, Yau WM, Tycko R (2004) Solid state NMR reveals a pH-dependent antiparallel beta-sheet registry in fibrils formed by a beta-amyloid peptide. J Mol Biol 335:247–260

53. Petkova AT, Leapman RD, Guo Z, Yau WM, Mattson MP, Tycko R (2005) Self-propagating, molecular-level polymorphism in Alzheimer's beta-amyloid fibrils. Science 307:262–265

54. Serpell LC (2000) Alzheimer's amyloid fibrils: structure and assembly. Biochim Biophys Acta 1502:16–30

55. Nilsberth C, Westlind-Danielsson A, Eckman CB, Condron MM, Axelman K, Forsell C, Stenh C, Luthman J, Teplow DB, Younkin SG, Näslund J, Lannfelt L (2001) The 'Arctic' APP mutation (E693G) causes Alzheimer's disease by enhanced Abeta protofibril formation. Nat Neurosci 4:887–8893

56. Murakami K, Irie K, Morimoto A, Ohigashi H, Shindo M, Nagao M, Shimizu T, Shirasawa T (2003) Neurotoxicity and physicochemical properties of Aβ mutant peptides from cerebral amyloid angiopathy: implication for the pathogenesis of cerebral amyloid angiopathy and Alzheimer's disease. J Biol Chem 278:46179–46187

57. Biancalana M, Koide S (2010) Molecular mechanism of Thioflavin-T binding to amyloid fibrils. Biochim Biophys Acta 1804:1405–1412

58. Wu C, Scott J, Shea JE (2012) Binding of Congo red to amyloid protofibrils of the Alzheimer Aβ(9–40) peptide probed by molecular dynamics simulations. Biophys J 103:550–557

59. Groenning M, Olsen L, van de Weert M, Flink JM, Frokjaer S, Jorgensen FS (2007) Study on the binding of Thioflavin T to beta-sheet-rich and non-beta-sheet cavities. J Struct Biol 158:358–369

60. Biancalana M, Makabe K, Koide A, Koide S (2009) Molecular mechanism of Thioflavin-T binding to the surface of beta-rich peptide self-assemblies. J Mol Biol 385:1052–1063

61. Klunk WE, Pettegrew JW, Abraham DJ (1989) Quantitative evaluation of Congo red binding to amyloid-like proteins with a beta-pleated sheet conformation. J Histochem Cytochem 37:1273–1281

62. Krebs MR, Bromley EH, Donald AM (2005) The binding of thioflavin-T to amyloid fibrils: localisation and implications. J Struct Biol 149:30–37

63. Chattopadhyay A (2003) Exploring membrane organization and dynamics by the wavelength-selective fluorescence approach. Chem Phys Lipids 122:3–17

64. Demchenko AP (1982) On the nanosecond mobility in proteins: edge excitation fluorescence red shift of protein-bound 2-(p-toluidinylnaphthalene)-6-sulfonate. Biophys Chem 15:101–109

65. Chattopadhyay A, Mukherjee S (1999) Red edge excitation shift of a deeply embedded membrane probe: implications in water penetration in the bilayer. J Phys Chem B 103:8180–8185

66. Nelson R, Sawaya MR, Balbirnie M, Madsen A, Riekel C, Grothe R, Eisenberg D (2005) Structure of the cross-beta spine of amyloid-like fibrils. Nature 435:773–778

67. Reddy G, Straub JE, Thirumalai D (2010) Dry amyloid fibril assembly in a yeast prion peptide is mediated by long-lived structures containing water wires. Proc Natl Acad Sci U S A 107:21459–21464

68. Zheng J, Jang H, Ma B, Tsai C, Nussinov R (2007) Modeling the Alzheimer Aβ$_{17-42}$ fibril architecture: tight intermolecular sheet-sheet association and intramolecular hydrated cavities. Biophys J 93:3046–3057

69. Dobretsov GE, Syrejshchikova TI, Gryzunov YA, Yakimenko MN (1998) Quantification of fluorescent molecules in heterogeneous media by use of the fluorescence decay amplitude analysis. J Fluoresc 8:27–33

70. Sarkar N, Das K, Nath DN, Bhattacharyya K (1994) Twisted charge transfer process of Nile Red in homogeneous solution and in faujasite zeolite. Langmuir 10:326–329

71. Togashi DM, Ryder AG (2006) Time-Resolved fluorescence studies on bovine serum albumin denaturation process. J Fluoresc 16:153–160

72. Stsiapura VI, Maskevich AA, Kuzmitsky VA, Uversky VN, Kuznetsova IM, Turoverov KK (2008) Thioflavin T as a molecular rotor: fluorescent properties of thioflavin T in solvents with different viscosity. J Phys Chem B 112:15893–15902

73. Wu C, Wang Z, Lei H, Zhang W, Duan Y (2007) Dual binding modes of Congo red to amyloid protofibril surface observed in molecular dynamics simulations. J Am Chem Soc 129:1225–1232

74. Wu C, Bowers MT, Shea JE (2011) On the origin of the stronger binding of PIB over thioflavin T to protofibrils of the Alzheimer amyloid-β peptide: a molecular dynamics study. Biophys J 100:1316–1324

75. Wolfe LS, Calabrese MF, Nath A, Blaho DV, Miranker AD, Xiong Y (2010) Protein-induced photophysical changes to the amyloid indicator dye thioflavin T. Proc Natl Acad Sci U S A 107:16863–16868

76. LeVine H (1995) Thioflavine T interaction with amyloid β-sheet structures. Amyloid 2:1–6

77. Sabate R, Saupe SJ (2007) Thioflavin T fluorescence anisotropy: an alternative technique for the study of amyloid aggregation. Biochem Biophys Res Commun 360:135–138

78. Schütz AK, Soragni A, Hornemann S, Aguzzi A, Ernst M, Böckmann A, Meier BH (2011) The amyloid-Congo red interface at atomic resolution. Angew Chem Int Ed Engl 50:5956–5960